ON THE PROPERTIES AND ORIGIN OF KUIPER BELT OBJECT ARROKOTH'S LARGE MOUNDS.

S.A. Stern[1], (astern@swri.edu), O.L. White[2,3], W.M. Grundy[4], B.A. Keeney[1], J.D. Hofgartner[1], W.B. McKinnon[5], D. Nesvorný[1], D.C. Richardson[6], J.C. Marohnic[6], A.J. Verbiscer[1], S.D. Benecchi[7], P.M. Schenk[8], J.M. Moore[3], K.D. Runyon[7]. [1]Southwest Research Institute, Boulder, CO 80302. [2]SETI Institute, Mountain View, CA, 94043. [3]NASA Ames Research Center, Moffett Field, CA, 94035. [4]Lowell Observatory, Flagstaff, AZ 86001. [5]Dept. Earth & Planetary Sci. and McDonnell Center for Space Sci., Washington U. in St. Louis, St. Louis, MO 63130. [6]Astronomy Dept, U. Maryland, College Park, MD 20742. [7]Planetary Science Institute, Tucson, AZ 85719, [8]Lunar and Planetary Science Institute, Houston, TX 77058.

Introduction. We report on a study of the large, prevalent mounds that dominate the appearance of Kuiper Belt Object (KBO) (486958) Arrokoth's larger lobe. We review the geological context of these mounds, their shapes, sizes and orientations, their reflectance, and their colors. We find the mounds are broadly self-similar in many respects, and interpret them as building blocks of the KBO.

Geologic Mapping of Wenu, Arrokoth's Large Lobe. Two geologic maps have already been produced for Arrokoth [1,2]; this new version makes improvements by using all available New Horizons (NH) data and also prioritizes stereo imaging between the CA06 (Closest Approach 06, 32.5° phase, 33 m/pixel) and CA04 (12.9° phase, 138 m/pix) observations, to more confidently identify contacts between mounds on Wenu, Arrokoth's larger lobe. Fig. 1b is our latest geologic map overlaying image CA06.

Contacts between mounds are easier to identify close to the terminator, where they often appear as troughs, scarps, and pit chains. Contacts are harder to identify nearer the limb; they are commonly identified by notches on the limb (which is especially evident in CA04), from which extends an usually faint lineation towards the center of the lobe face. Some contacts are enhanced by a stretch of bright material, interpreted to be loose regolith that has accumulated in a valley between mounds that defines the contact.

Twelve mounds have been identified; they appear to be organized such that smaller mounds (units *ta-tk*) cluster around a large central mound (unit *tl*). Wenu is estimated to be only ~10 km thick, implying that these mounds, most of which are >5 km wide, likely extend all the way through the body of the lobe to the far side not seen by NH. The fact that the inertial axis of the large lobe is located within mound *tl*, implies that the smaller mounds later accreted around the equator of mound *tl* to build up the large lobe. A stratigraphic sequence of mound accretion, indicated by the numbers next to the mound labels in Fig. 1b, has been derived based on crosscutting relations (T-junctions) of mound contacts, the convexity of contacts, and the topographic prominence of mounds as expressed by the angularity of their limb profiles. Mounds with a number higher than that of a mound bordering it accreted later.

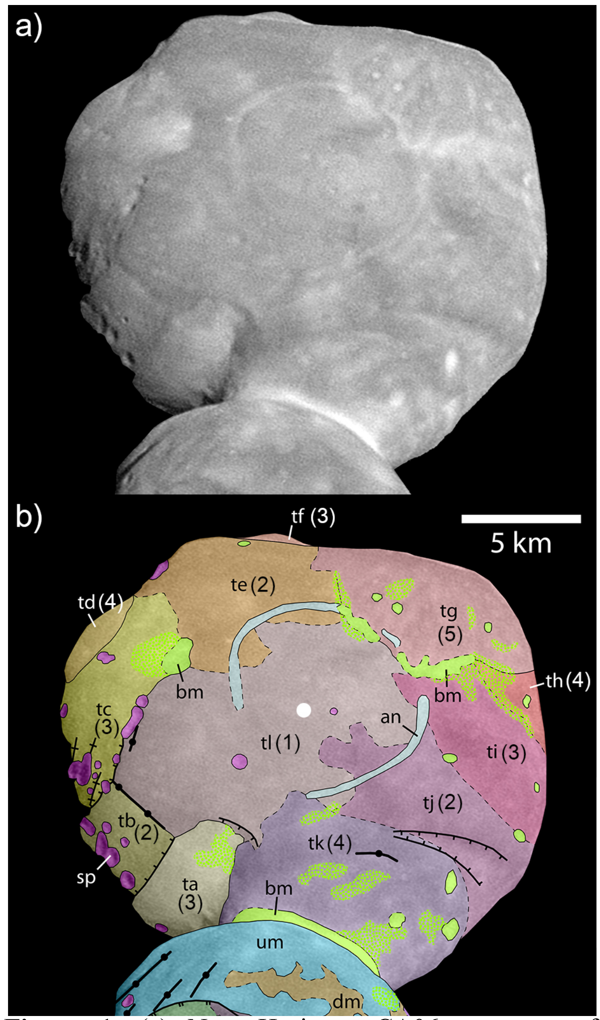

Figure 1. (a) New Horizons CA06 coverage of Arrokoth's Wenu lobe. (b) Same coverage with geological map overlain. The 12 mounds are mapped as units *ta* through *tl*. Bright material is mapped as *bm*. White dot is the approximate inertial axis of Wenu [3].

Mound Shapes and Sizes. Three of Wenu's mounds *(td, tf,* and *th*) are observed obliquely in the CA06 observation. The rest have observed areas that range between 9.3±0.6 km^2 (*tb*) and 69±1 km^2 (*tl*), and all but *tk* and *tl* have observed areas within a factor of ~3 of one another (Fig. 2). The observed aspect ratios of the mounds with good visibility range from 1.3±0.1 (*tb*) to 2.7±0.1 (*tc*); i.e., within a factor of ~2 of one another. The remarkably consistent properties across the mounds, suggest that the subunits that merged to form Wenu had broadly similar shapes and sizes.

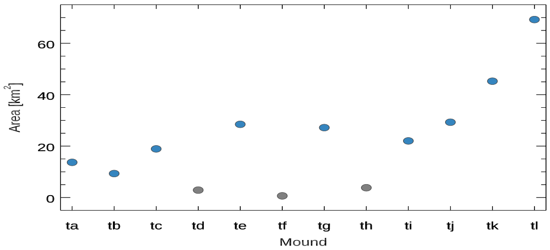

Figure 2. Observed area of the mounds in the NH CA06 observation, uncorrected for projection effects. Well-observed mounds in blue; those with poor visibility in gray; uncertainties are smaller than symbol sizes.

Photometry. The photometry of Arrokoth's mounds has been investigated using a previously published normal reflectance map [10]. Fig. 3 shows the normal reflectance cumulative probability for 10 mounds (*td* and *tf* are not included because of their small areas). All of Wenu's mounds have similar normal reflectance distributions. Subtle differences between mounds are noted. Mounds *ta-tc* have slightly greater normal reflectance standard deviations than the other mounds, which is due to their location near the terminator where errors of the normal reflectance map are largest. Mound *tb* has the least Gaussian distribution, attributed to a darker than average area near its boundary with mounds *ta* and *tl.* Mounds *tg* and *th* have a slightly greater normal reflectance mode than the other mounds, which may be related to their suggested later emplacement.

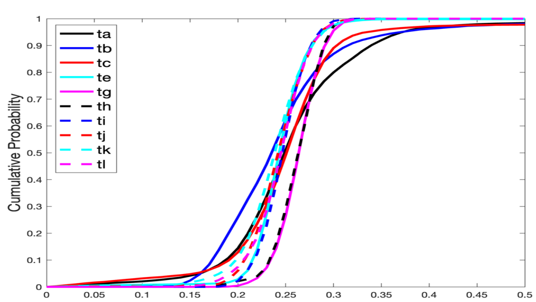

Figure 3. Cumulative normal reflectance distributions of 10 largest (i.e., most aerially extensive) mounds.

Colors. New Horizons' best MVIC color observation was CA05, obtained between the panchromatic CA04 and CA06 observations. The image scale was 340 m/pixel, though the actual resolution was coarser owing to the point spread function and changing spacecraft-target geometry during the observation. Regions of interest (ROIs) were selected to exclusively sample each of the larger mounds, avoiding regions near the limb or mound boundaries where image smear could produce pixels contaminated by sky or another mound.

A comparison of color ratios among ROIs shows the mounds are mostly similar to one another in terms of average color and also color distribution (mean NIR/RED I/F color ratios 1.49 to 1.51 with a variance of 0.03), but three mounds stand out for colors distinct from the others. The most different is *ta*, which is less red than the others (NIR/RED ratio 1.39). However, *ta's* proximity to the neck region suggests its distinct color could be associated with whatever process is responsible for the bright neck. Mound *te* is slightly redder (NIR/RED ratio 1.53). The color difference appears to be intrinsic to mound *te*, rather than the result of subsequent modification. The last mound exhibiting distinctive colors is *tj* which has a broader color distribution as indicated by a variance of 0.05. The main area of *ta* is slightly redder (NIR/RED ~1.52) than the trough along the bottom of *tj* in Fig. 1b which is somewhat less red, though not as extreme as *ta.*

On Origins. The individual mapped units on Wenu indicate the merger or assembly of discrete multi-km-scale planetesimals. If so, to create such a lenticular or ellipsoidal body as Wenu requires that the mergers were themselves not very energetic or high velocity [4]. These velocity conditions would have been met in a collapsing particle cloud, such as created in the solar nebula midplane by the streaming instability [4-8], but not during heliocentric hierarchical coagulation generally. Preliminary calculations of collisional mergers between ~3-5-km diameter bodies indicate that normal impact speeds $\lesssim$1 m/s are necessary to preserve the shapes of the individual subunits, using the same "gravel" friction parameters as in [9].

A major question remains: Why did a set of broadly similar ~3-5-km diameter mound-forming bodies assemble to form Wenu, as opposed to a hierarchy of sizes, or simply a vast assembly of small pebbles? The highest resolution pebble cloud evolution study to date [8] shows clouds collapsing to dense, rotating disks, followed by spin up and mass loss to spiral arms. Determining whether a characteristic planetesimal building-block size emerges will require even greater resolution. Wenu is an oblate but not obviously triaxial body, and its flattening (~0.55 [3]) is consistent with a primordial (pre-contact-binary) rotation period of 11.5 (8.1) hr for a uniform density of 250 (500) kg/m^3.

References. [1] Stern S.A.+ (2019) *Science 364*, eaaw9771. [2] Spencer J.R.+ (2020) *Science 367*, eaay3999. [3] Keane J.T.+ (2022) *JGRE 127*, e07068. [4] McKinnon W.B.+. (2020) *Science 367*, eaay6620. [5] Nesvorný D.+ (2010) *AJ 140*, 785–793. [6] Fraser W.C.+ (2017) *Nature Astron. 1*, 0088. [7] Robertson J.E.+ (2020) *A&A 643*, A55. [8] Nesvorný D.+ (2021) *PSJ 2*, 27. [9] Marohnic J.+ (2021) *Icarus 356*, 113824. [10] Hofgartner J.D.+ (2021) *Icarus, 356,* 113723.